JTTEE5 8:565-575

Effect of Nozzle Configuration, Gas Pressure, and Gas Type on Coating Properties in Wire Arc Spray

X. Wang, J. Heberlein, E. Pfender, and W. Gerberich

(Submitted 15 Oct 1998; in revised form 19 May 1999)

Wire arc spraying is a coating process in which minor modifications of the configuration and spray parameters can have a strong impact on coating characteristics. A study on the effects of the fluid dynamics of the atomizing gas on the coating properties is presented. Different types of nozzles, shrouds, and gases have been used to provide various flow velocities and reactive environments in the metal atomization region. The effects on particle velocity, coating density, composition, and interface characteristics between the coating and the substrate have been evaluated. It is clear that higher gas velocities improve practically all coating properties, but also increase oxide content in the coating. However, the oxidation can be drastically reduced if nonoxidizing gases are used for atomization in combination with a shroud. A discussion on the physical effects contributing to the observed adhesion improvements and interfacial properties is provided.

Keywords adhesion, coatings, nozzles, porosity, wire arc spraying

1. Introduction

Wire arc spraying is an efficient and economical coating technique, which has a wide range of applications in industry (Ref 1-3). Some of its principal attractions are its operational simplicity and the low cost for the wire feedstock. However, this simplicity does not exclude that minor modifications of the equipment design features can strongly influence the coating properties. Because of the resurgent interest in this process, a number of new developments in improving the equipment have been initiated and introduced. This is particularly true for the way the atomizing gas is delivered to the wire tips. In the wire arc spray process, the arc between the tips of two continuously advancing wires melts the material, and the molten metal is removed and blown toward the substrate by a high-velocity gas stream. This gas stream is responsible for forming the initial droplets after removal of the molten material from the wire tips (primary breakup), for atomizing the larger droplets (secondary breakup), and for accelerating them toward the substrate. Higher gas velocities will result in the generation of finer droplets, which are accelerated to higher velocities. A detailed description of these effects has been presented by Steffens (Ref 4).

In this article, the results of a systematic investigation of the influence of different nozzle and shroud configurations on the coating properties is presented, including the effects on particle size distribution, particle velocities, coating microstructure and composition, and coating adhesion. The nozzle configurations investigated are shown schematically in Fig. 1 and can be characterized as follows: A is the standard nozzle with a straight bore, B is a converging-diverging nozzle allowing supersonic flow of the atomizing gas to extend farther into the atomizing region, C is a standard nozzle with secondary gas injection, and D

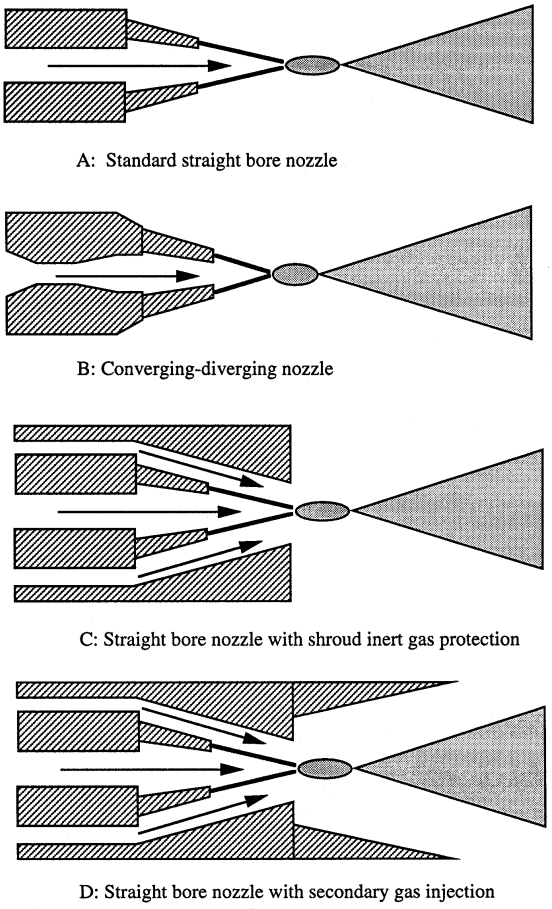

Fig. 1 Schematic of nozzle configurations

X. Wang, J. Heberlein, E. Pfender, and **W. Gerberich,** ERC for Plasma-Aided Manufacturing, University of Minnesota. Contact e-mail: jvrh@me.umn.edu.

represents the addition of a shroud to the nozzle with secondary gas injection. Each of these arrangements has different fluid dynamic features, and results obtained with each of them are presented.

2. Experimental Methods

2.1 Process Conditions

Before spraying, the substrates were treated by grit blasting, acetone degreasing, and ultrasonic cleaning. A Metco (Sulzer Metco U.S. Inc., Westbury, NY) 4RG gun was used; Table 1 lists the operating conditions. For all the cases, the arc voltage, current, and standoff distance were set at 30 V, 150 A, and 15 cm, respectively. In cases A and B, aluminum was sprayed onto a steel substrate, while in cases C and D, stainless steel was sprayed onto an aluminum substrate.

Table 1 Operating conditions

Nozzle configuration	Gas pressure, psi	Gas flow rate, scfm	Gas type
A	45, 65, 85	9, 13, 17	Air
B	65	15	Air
C	Primary: 60 Secondary: 15	Primary: 12 Secondary: 3	Air Air
D	Primary: 60 Secondary: 15	Primary: 12 Secondary: 3	Carbon dioxide, nitrogen

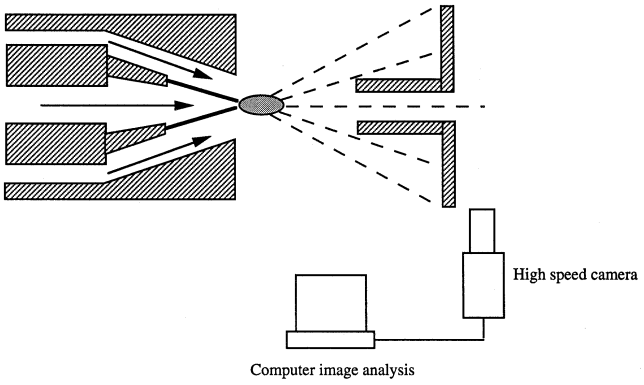

Fig. 2 Experimental setup for particle velocity measurements

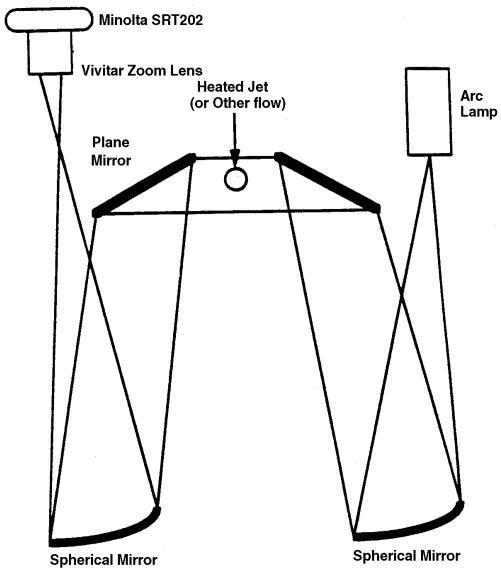

Fig. 3 Experimental setup for shadowgraph measurement

2.2 Measurement of Gas Velocity and Particle Velocity

A Pitot tube was used to measure the gas velocity at the nozzle exit. In incompressible flow, the Bernoulli equation can be used to relate changes in velocity and pressure along the streamline when the flow is not affected by friction:

$$P_0 = P + \left(\frac{1}{2}\right)\rho V^2$$

where P_0 is the stagnation pressure, P is the static pressure at a point in the flow where the velocity is V, and ρ is the gas density. Thus, measurement of the stagnation pressure and the static pressure will yield the gas velocity (Ref 5).

Images of particle streaks were taken with a Kodak high-speed vision system (Eastman Kodak, Rochester, NY). The exposure time was adjusted until clear particle streaks could be recorded. The streak length was then determined using image analysis and divided by the exposure time, thus giving particle velocity. About 40 images were evaluated to obtain average particle velocities. For these measurements, using a diaphragm reduced the metal droplet density in the stream. Figure 2 shows the experimental setup for the particle velocity measurements.

2.3 Gas Stream Visualization

A shadowgraph setup, as shown in Fig. 3, was used to study the gas flow (Ref 6). A mercury arc lamp with a 2 mm diameter aperture was the point light source. The light was collimated using a 21.6 cm diameter spherical mirror with a focal length of 168 cm. A plane mirror turned the light by 90° to pass through the flow. The light was again turned 90° by a plane mirror and focused to a point by an identical spherical mirror. A Vivitar (Vivitar Corp., Newbury Park, CA) zoom lens with a fully open aperture was used to focus the light onto the film. A shutter speed of $^1/_{1000}$ s and 400 ASA black and white film were used to produce the images shown in Fig. 7 (Ref 6).

2.4 Coating Microstructure and Composition Analysis

Micrographs of polished coating cross sections were investigated using reflected light microscopy with a green filter for improved contrast at 200× magnification. Scanning electron microscopy (SEM) was used to examine the cross sections of the samples and microfractography. The surface morphology of coatings was also studied by SEM. Energy dispersive x-ray analysis was used for determining composition of the interfacial region and fracture surfaces. Auger electron spectroscopy is a nondestructive technique with a sensitive depth resolution suitable for elemental analysis of materials. To eliminate surface contamination, the sample surface was etched to a depth of 300

Å by argon ion beam sputtering. The atomic concentrations were calculated from the intensity of the Auger peaks based on a calibration of relative sensitivity. Chemical composition profiles were taken using a scanning Auger microprobe to study the film-substrate interfacial chemistry. On a perpendicular section of the coated sample, a linear scan along the direction orthogonal to the boundary surface was taken to determine concentration profiles of the elements in the film and substrate. X-ray diffraction with CuKα radiation was used for identification of the intermediate phases formed at the interfacial region and oxide phase of coatings.

2.5 Porosity and Particle Size Measurement

Image analysis was used to determine the porosity of polished coating cross sections. The analysis used differences in gray levels to distinguish different features of the coating microstructure. Features such as porosity were detected through their respective gray scale ranges, and pore sizes were measured. The porosity measurements were performed for 12 different locations randomly distributed over the coating cross sections to obtain average results. Droplet size was determined by spraying into ice and observing the resulting solidified particles with SEM combined with image analysis.

2.6 Adhesive Bond Strength Test

The bond strength of coatings was measured in accordance with the ASTM C 633-79 standard pull-off tensile test. This is a common method of characterizing the comparable bond strength of thermally sprayed coatings. The results of the tests determine the degree of adhesion of a coating to a substrate in tension normal to the surface. Twelve tests were performed on each sample using an Instron machine (Instron Corp., Canton, MA) at a crosshead speed of 0.075 cm/min.

2.7 Microhardness Test

A Vickers microhardness indenter was employed to measure Vickers hardness profiles across the coating-substrate interface. Measurements were made using a load of 200 g for 10 s. On each sample, twelve measurements were made at random locations.

3. Results and Discussion

3.1 Effect of Atomizing Gas Pressure and Flow Rate on Coating Properties with the Straight Bore Nozzle

Arc fluctuations due to periodic removal of molten droplets from the wire tips by the atomizing gas stream are characteristic for the wire arc spraying process (Ref 2, 4, 7-10). Dynamic forces of the atomizing air stream acting on the arc as well as on the droplets lead to different particle sizes, which, in turn, determine porosity and oxide content of sprayed coatings. In this study, arc spraying of aluminum coatings was considered with the objective of establishing correlations between atomizing air pressure and coating properties such as porosity and oxide content.

Droplet Formation from the Wire Tips and Droplet Size Distributions. Figure 4 shows a high-speed photograph of an asymmetric melting behavior of the cathode and the anode wire. The anode melts slowly, resulting in elongated relatively large droplets. This uneven melting leads to an asymmetry of the arc and affects the spray pattern and the coating structure. At the cathode, melting is more localized, and the molten droplets are immediately blown away by the atomizing gas flow, resulting in relatively small droplets. The higher melting rate at the cathode is due to a more constricted arc attachment compared to the more diffuse arc attachment at the anode. From sequences of high-speed videographs, it is apparent that higher atomizing air pressures result in smaller droplet sizes. This fact has been corroborated by measurement of the particle size distributions, shown in Fig. 5.

Oxide Content of the Coating. Arc sprayed metal coatings contain a certain amount of oxides. A quantitative analysis using Auger electron spectroscopy (AES) revealed that the amount of aluminum oxide in the coating increased with increasing atomizing air pressure. The amount of oxide content calculated from the peak intensity of the AES in the coatings has been 18.2 (±1.6), 19.5 (±1.9), and 24.8% (±2.1%) as the gas pressure increased from 0.31 to 0.45 MPa and to 0.59 MPa, respectively. During spraying, the effect of atomizing air and the entrainment of the surrounding air into the spray stream caused significant inflight oxidation of the molten metal particles (Ref 11). Increasing the atomizing air pressure leads to higher gas stream velocities, which in turn break up the molten particles into smaller droplets. The smaller droplets react more readily with oxygen than the larger droplets, because of their greater specific surface area. Thus, coatings sprayed under higher atomizing air pressure tend to exhibit a higher oxide content.

Coating Porosity. Figure 6 shows polarized optical micrographs of cross sections of sprayed coatings. Using computerized image analysis, the porosity of the coatings has been determined quantitatively. The porosity of the coatings is 27 (±4), 18 (±4), and 12% (±3%) for gas pressures of 0.31, 0.45, and 0.59 MPa, respectively, indicating that the gas pressure is an important parameter in terms of porosity. The sprayed coating is built up particle by particle and, therefore, higher atomizing air pressure results in higher impact velocity of smaller particles on the substrate. Faster molten particles with higher kinetic energy spread and deform more readily on impact, thus increasing coating density and reducing porosity.

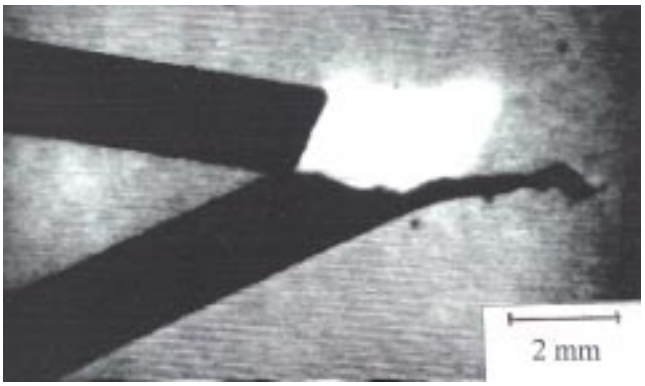

Fig. 4 High-speed image of droplet formations

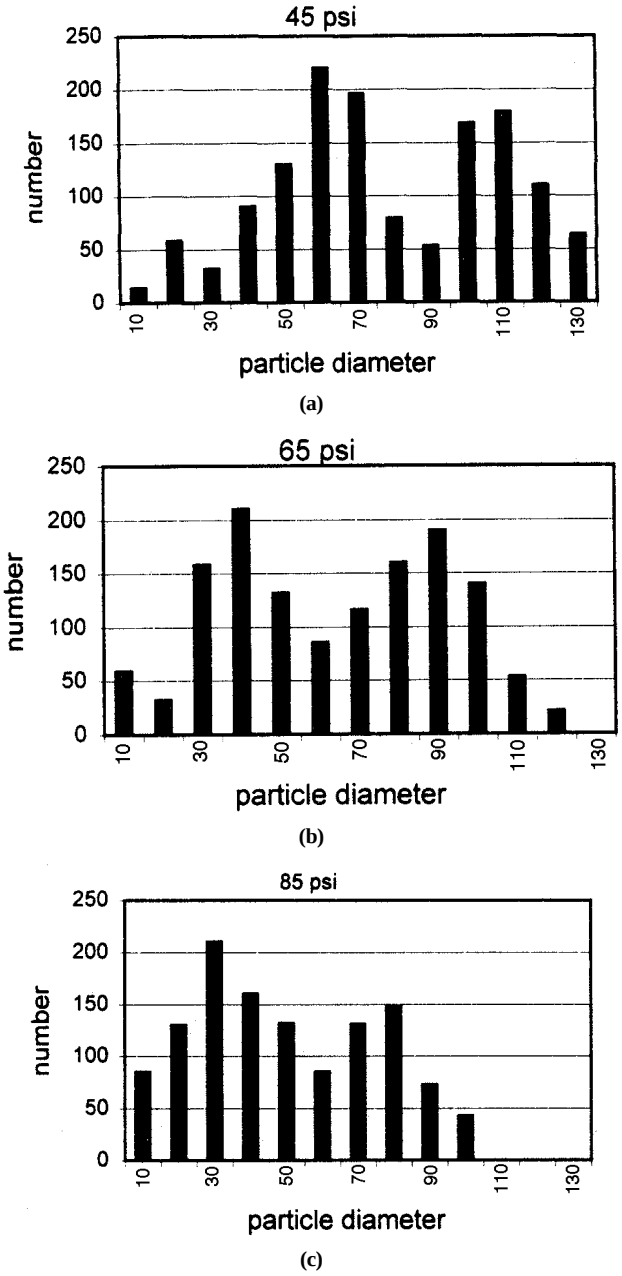

Fig. 5 Aluminum particle size distributions. (a) 0.31 MPa. (b) 0.45 MPa. (c) 0.59 MPa

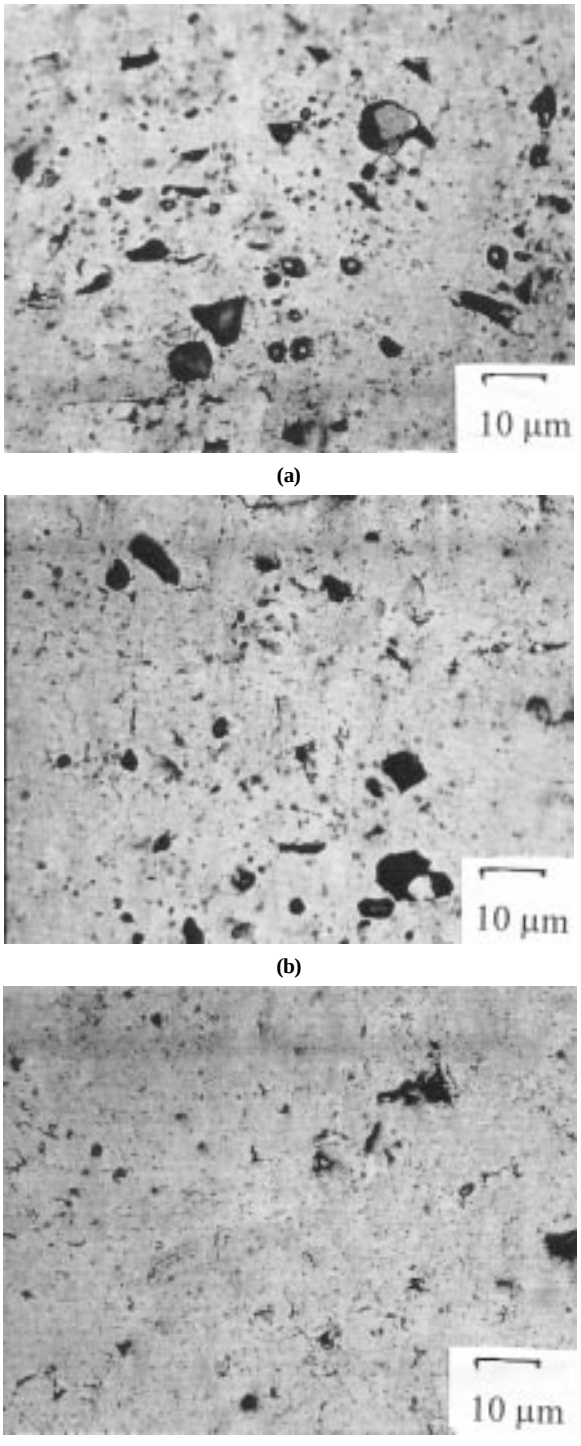

Fig. 6 Micrographs of coating cross sections. (a) 0.31 MPa. (b) 0.45 MPa. (c) 0.59 MPa

3.2 Effect of Converging-Diverging Nozzle on Coating Properties

To produce coatings with high density and high bond strength, a converging-diverging atomizing gas nozzle (CD nozzle) was used to accelerate the gas jet to supersonic levels without choking, thus increasing particle velocity (Ref 12). To achieve better corrosion and wear resistance, coatings with minimal porosity and maximum strength are required. However, the velocities of the particles are subject to certain limitations. Coatings produced with conventional nozzles have relatively high porosity and relatively low bond strength. Increasing the atomizing gas speeds to supersonic velocities by properly expanding the flow in a converging-diverging nozzle as opposed to the conventional straight bore nozzle is expected to improve coating density and adhesion. The converging-diverging nozzle is shown schematically in Fig. 1(b). The nozzle throat-to-exit area ratio is matched to the required pressure ratio for the conditions of Mach number 1.5.

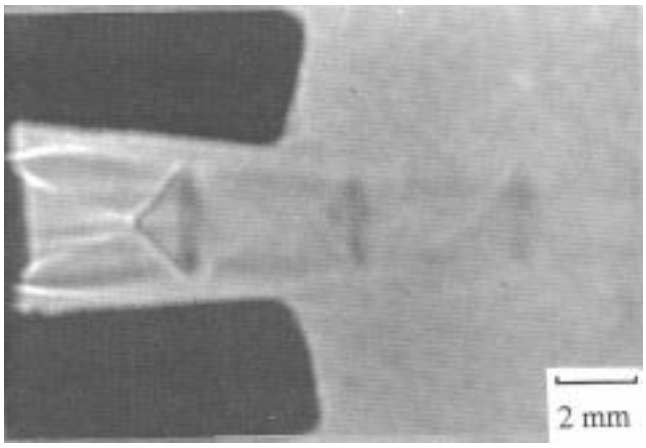

(a)

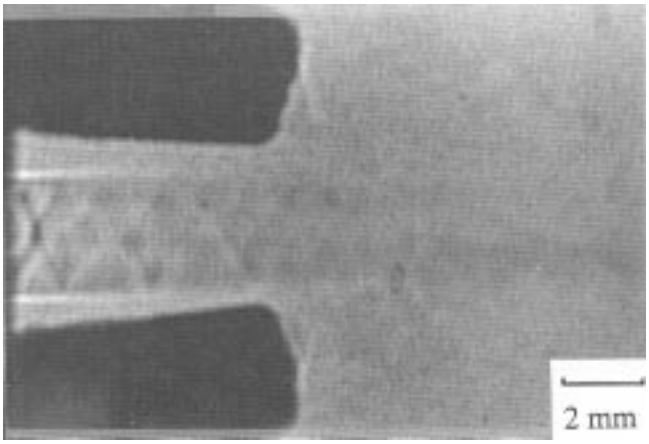

(b)

Fig. 7 Shadowgraphs of gas flow pattern. (a) Conventional straight bore nozzle. (b) Converging-diverging nozzle

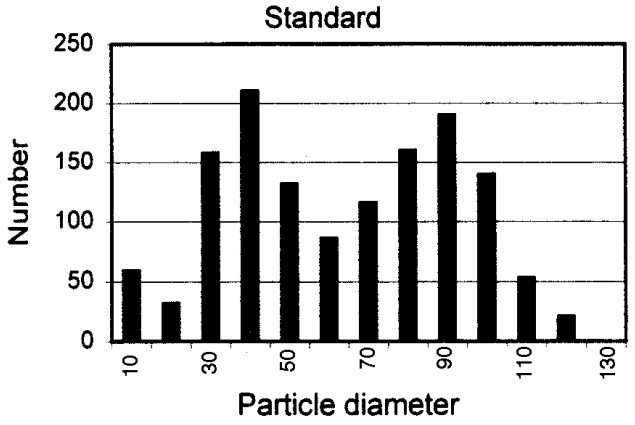

(a)

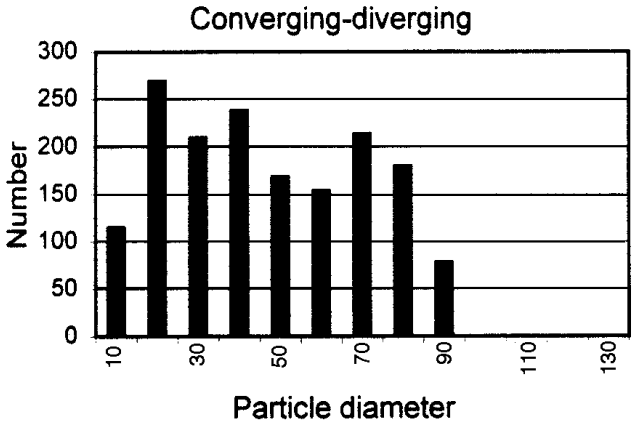

(b)

Fig. 8 Particle size distributions. (a) Conventional straight bore nozzle. (b) Converging-diverging nozzle

Flow Patterns of Atomizing Gas Stream. Figure 7 shows shadowgraphs of gas streams produced by the CD nozzle and a conventional nozzle. Visualization of the atomizing gas stream produced with a straight bore nozzle illustrates the formation of a strong shock structure and nonuniformity. This effect causes rapid velocity decay. In contrast, the gas stream produced with a CD nozzle has a very weak shock structure and a visually longer high velocity potential core. Because the gas stream drives the molten particles, the associated molten particle velocities are increased as well.

Particle Size Distribution. Figure 8 shows particle size distributions for two different nozzles. For both conditions the particles have a bimodal size distribution. This distribution is likely the result of the difference in size of the initial droplets from the anode and the cathode. But it is obvious that the higher gas velocities of the converging-diverging nozzle lead to smaller particles with a narrower distribution.

Coating Microstructure. The particle velocity and the particle temperature determine the coating structure at the instant of impact on the substrate. Completely molten particles impinging on the substrate spread out radially in the form of thin disks. In reality, however, the deposit is not uniform in thickness, and the periphery of the flattened particle is not circular. Figure 9 shows the surface morphology of aluminum coatings prepared with the CD nozzle and a conventional nozzle. It is obvious that the flattening behavior is different for the two cases. The molten particles sprayed with the CD nozzle spread out to a much greater extent than those sprayed with the conventional nozzle. They also show a higher degree of deformation, and there are fewer unmolten droplets at the edges of the flattened particles. Figure 10 shows cross-sectional views of aluminum coatings sprayed with the CD nozzle and the conventional nozzle illustrating that the coatings prepared with the CD nozzle have lower porosity than those produced with the conventional nozzle. Also, the pore sizes of the coatings obtained with the CD nozzle are in general smaller than those of the coatings obtained with the conventional nozzle.

The higher velocity of the atomizing gas stream obtained with a converging-diverging nozzle readily explains these observations. In wire arc spraying, the particle has its highest temperature in front of the wire electrode, and a higher atomizing gas velocity will lead to higher particle acceleration. The consequence is not only a higher impact velocity, but also a higher particle temperature at impact because of the shorter flight time and less cooling by entrained air. The higher temperatures result in lower viscosities and better wettabilities, yielding better conformal coatings in the case of using the CD nozzle (Ref 13).

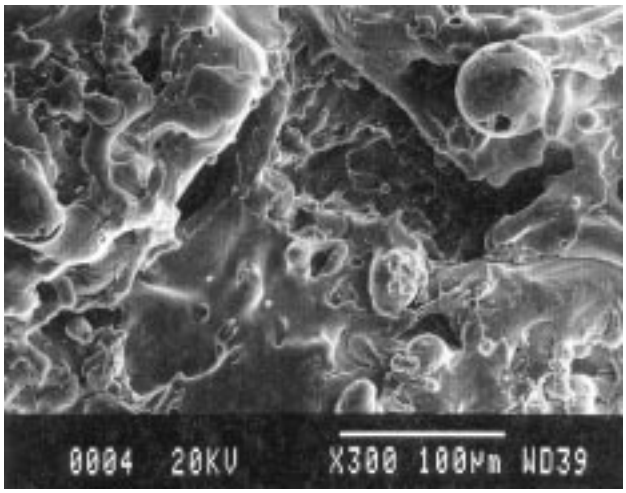

(a)

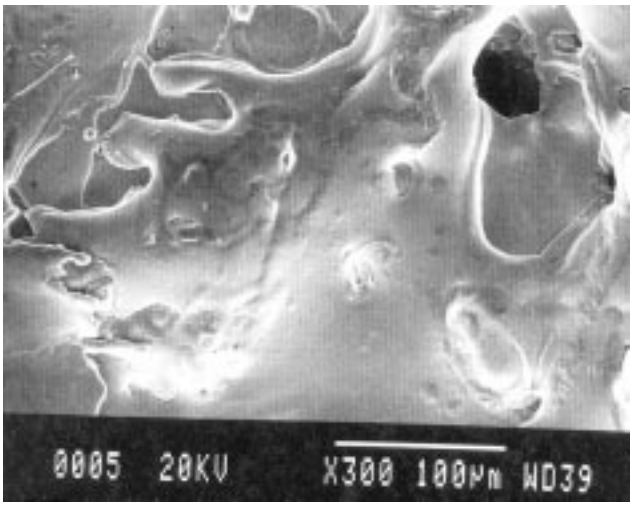

(b)

Fig. 9 Surface morphology of coatings. (a) Conventional straight bore nozzle. (b) Converging-diverging nozzle

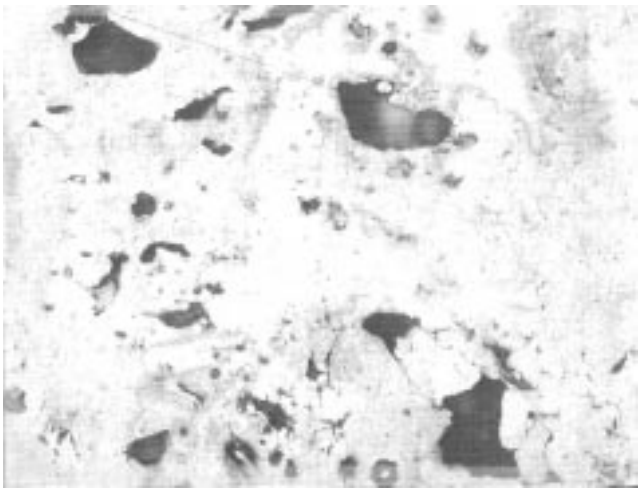

(a)

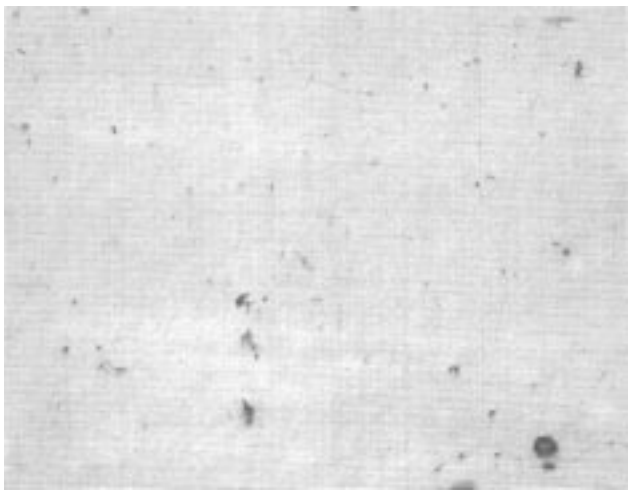

(b)

Fig. 10 Micrographs (200×) of cross sections of a coating under two conditions. (a) Conventional straight bore nozzle. (b) Converging-diverging nozzle

Coating Properties. A significant criterion for the quality of thermally sprayed films is their adhesion to the substrate. The coating is built up particle by particle. Molten particles undergo severe deformation and rapid solidification when they impinge on the substrate. To achieve high bond strength between film and substrate, the particles must be in a fully molten state and have sufficient velocities to be able to spread out and flow into the contours and crevices of the roughened substrate. The results of adhesion tests indicate that the bonding strength of the aluminum coating sprayed with the CD nozzle (about 35 MPa) is higher than that sprayed with the conventional nozzle (about 20 MPa), as shown in Table 2.

Microhardness is of interest because it gives an indication of resistance to abrasive wear. It is greatly affected by the amount of oxide and porosity of the deposit. The coating with more pores has less resistance to penetration than the denser coating, consequently displaying lower hardness. Conversely, oxide particles in the coating tend to give a higher hardness. The values for the microhardness cover a relatively wide range. This correlates with the large phase heterogeneity and porosity of the coatings.

3.3 Effect of Secondary Gas or Inert Gas on Coating Microstructure

Coating density and bond strength depend to a large degree on particle velocities. In conventional wire arc spraying, the velocities of the larger particles are relatively low, limiting the bond strength of the coating. Spraying with secondary gas atomization results in more uniform particle size distributions, more focused spray patterns, higher particle velocities, and improved coating properties. A modified nozzle with secondary gas injection as shown in Fig. 1(c) was used to optimize atomization and enhance particle velocities. A primary axial air stream removes the molten metal droplets from the wire tips and from the area of the wire intersection, and a secondary air stream forms a conical sheath around the axial air stream. The primary gas stream and the secondary gas stream emerge from the nozzle

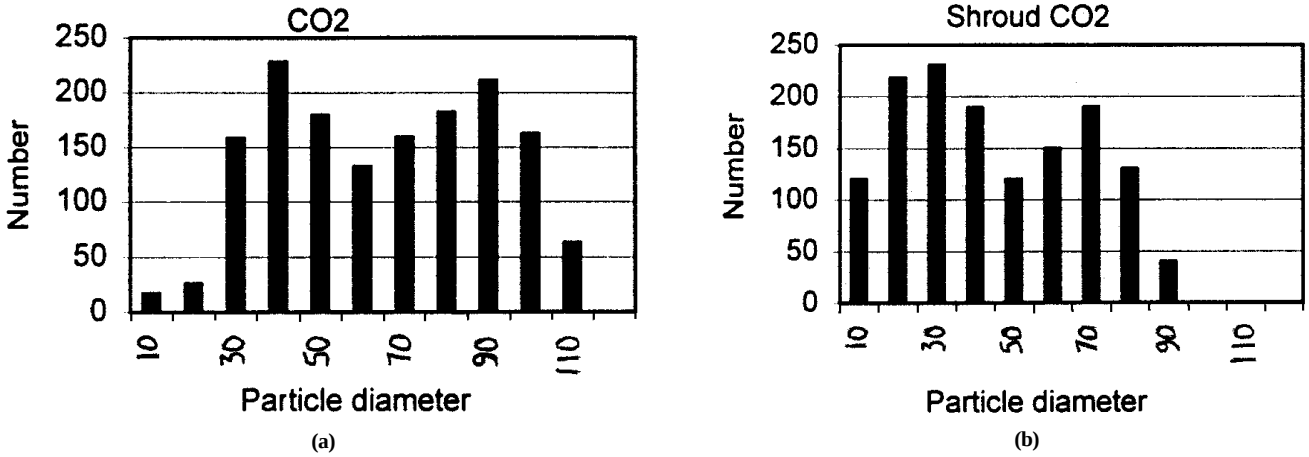

Fig. 11 Particle size distributions of stainless steel particles atomized with CO_2. (a) Nonshrouded. (b) Shrouded

Table 2 Bond strength and microhardness of aluminum coatings from different nozzles (12 measurements)

Nozzle type	Bond strength (mean), MPa	Bond strength (σ), MPa	Microhardness (mean), HV	Microhardness (σ), HV
Converging-diverging nozzle	35.4	7.1	59	11
Straight bore nozzle	20.2	6.2	51	9

as coaxial gas streams, thus tending to protect the droplets from entrained air and to concentrate the flow pattern of the droplets. Lower coating porosity and higher bond strength are expected from the secondary gas injection.

Air atomization is commonly used in the wire arc spray process. The major advantages are the availability and economy of compressed air. In the air atomization wire-arc spray process, the oxide content of the sprayed coating is relatively high due to oxidation of the molten wire material. This higher oxide content can increase the coating hardness so that the abrasion and wear resistance of the coatings is improved. However, the oxide content may also be detrimental to coating properties because oxides may reduce the adhesion strength between coating and substrate. Also, hard oxide particles embedded in sprayed coatings impose problems during machining. Furthermore, coatings sprayed with air atomization often contain relatively high porosity, which is frequently detrimental. Another disadvantage of air atomization is related to the burnoff of alloying elements (such as chromium and carbon) contained in parent wires. These elements are essential ingredients to produce the required coating characteristics. As a consequence, coatings with specified characteristics cannot be produced reliably. In this study, nitrogen and carbon dioxide have been used as atomizing gas in wire arc spraying to produce coatings with higher quality.

However, even spraying with nitrogen and carbon dioxide as atomizing gas may still result in strong oxidation of coatings because of entrainment of large amounts of air (Ref 11). Air entrainment can cause a strong drop of temperature and velocity of the gas stream. An obvious approach to avoid air entrainment is to shield the atomizing gas flow from the surrounding atmosphere by using a shroud.

Gas Velocity, Particle Size, and Particle Velocity. The measurements show that the gas velocity (610 ± 22 m/s) at the nozzle exit in the case of primary/secondary air atomization (Fig. 1c) is higher than that (530 ± 15 m/s) in the case of primary air atomization only (Fig. 1a). The atomization of the molten droplets is enhanced by secondary gas injection, which leads to smaller droplets, which are accelerated faster by the gas flow. Results of image analysis of high-speed photographs of particle flight trajectories indicate that in the case of secondary gas atomization, the average particle velocity is about 105 m/s (±10 m/s) when particles impact the substrate surface, while in the case of primary gas atomization, the particle velocity is about 70 m/s (±8 m/s).

Particle Size Distributions. Droplet size was determined by spraying into ice and analyzing the size distribution of the solidified particles with SEM and image analysis system. Assuming that all particles are captured by ice, the size distributions for particles sprayed with CO_2 as atomizing gas with and without shroud are shown in Fig. 11. There is a clear reduction in average particle size, but a bimodal distribution is observed in both cases. The smaller particles probably originate from the cathode, which has a more constricted attachment and higher atomization.

Coating Microstructure. Figure 12 shows scanning electron micrographs of cross sections of sprayed coatings. Using computerized image analysis, the porosity of the coatings was determined quantitatively. The porosity in the case of air atomization was 17% (±3%), which is higher than that in the case of CO_2 atomization (12 ± 2%) and N_2 atomization (13 ± 2%). The porosity in the case of gas shrouding was substantially reduced to 6% (±2%) for CO_2 atomization and 8% (±2%) for N_2. This can be explained by two factors: (a) The shrouded inert gas sprayed coatings result in the lowest oxide content; therefore, there is a more uniform contact between metallic splats, which makes the coating more consistent and less porous. (b) Because the shrouded nozzle with secondary inert gas injection leads to higher acceleration of the droplets and less cooling by the entrained air, the coating was built up by particles with higher velocity and temperature leading to the lowest porosity. Defects

were hardly seen in the deposited layer, and the structure was very fine when using shrouded nozzles with secondary inert gas atomization. In air sprayed coatings, many microcracks originated from oxide/metal interfaces due to the large amount of oxide embedded inside the coating. In the case of inert gas atomization, particularly in the case of shrouded inert gas atomization, fewer microcracks of the same size were observed. It is possible that there were more smaller microcracks, which have not been resolved, under these conditions. However, for the same SEM with the same magnification, more cracks were observed when using air sprayed coatings than shrouded inert gas sprayed coatings. This can be explained by the fact that less oxidation yields better conformal coatings.

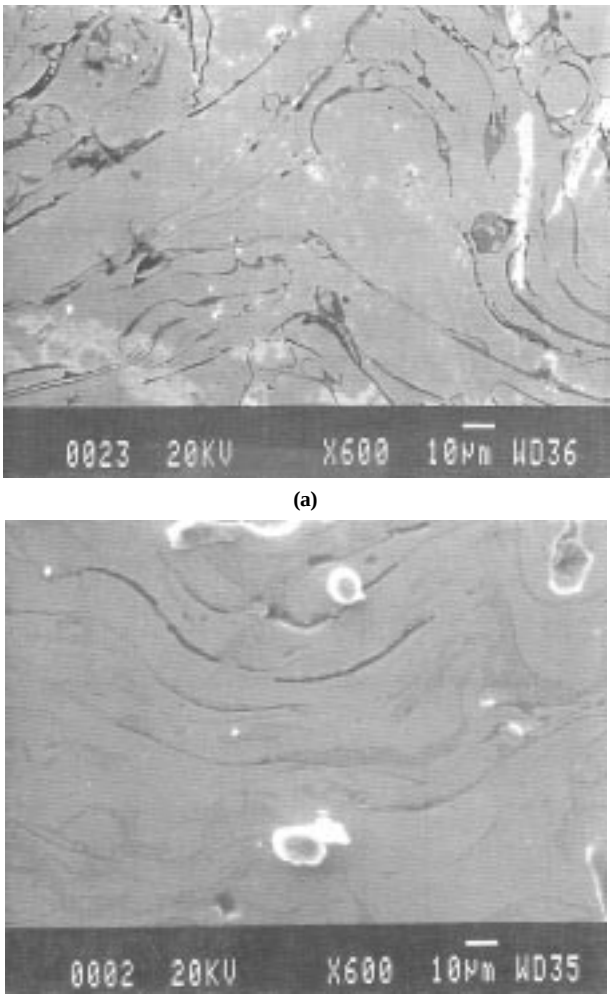

Fig. 12 Micrographs of coating cross sections. (a) Nonshrouded. (b) Shrouded

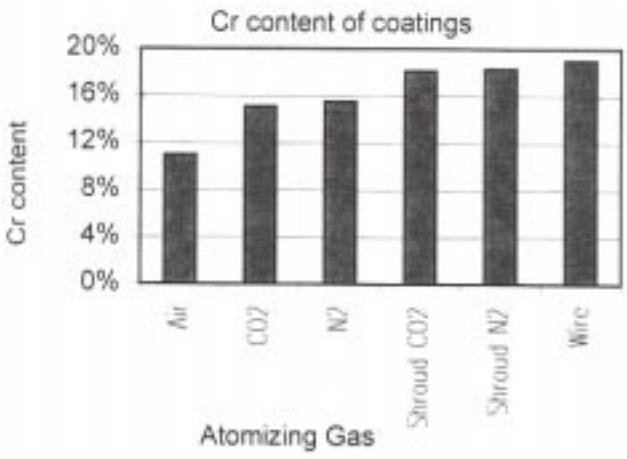

Fig. 13 Chromium content of stainless steel wire and coatings sprayed with different gases

Alloy Element Loss. Figure 13 shows the chromium content of the original stainless steel wire, and of the air, CO_2, and N_2 sprayed coatings tested by AES. The results indicate that when air is used as the atomizing gas, a significant amount of chromium is lost, as shown by the fact that the deposited coating contained 11 wt% (±2%) Cr compared with the wire having 19 wt% (±2%) Cr. The formation of CrO_3 by the reaction: Cr_2O_3 (s) + $^3/_2$ O_2 (g) → 2 CrO_3 (g) becomes significant at high temperatures (Ref 15), resulting in chromium loss by evaporation of CrO_3. Using a shrouded nozzle with secondary CO_2 or N_2 gas injection, the chromium content of the coating was essentially the same as that of the original wire. This indicates that the shrouded nozzle reduces the mixing of entrained air with the atomizing gas.

Oxide Content of the Coating. The amount of oxide depends on both the amount of oxygen present in the spraying jet and the total surface area of the particles in the jet. Figure 14 shows the oxide content. The amount of oxide in the air sprayed coating (21%) was higher than that of the inert gas sprayed coating, and the use of the shrouded nozzle with inert gas further decreased the oxide content. Using inert gas without a shrouded nozzle does not eliminate the oxides because of the entrainment of air from the surroundings (Ref 11). However, using a shrouded nozzle with secondary inert gas injection reduced the oxide content even though the particle size was decreased. This indicates that using a shrouded nozzle can result in coatings with both higher density and less oxide content.

3.4 Adhesion

Section 3.3 presents results showing narrower size distributions and denser coatings when secondary gas injection was used. Thus, higher bond strength is expected to be obtained with

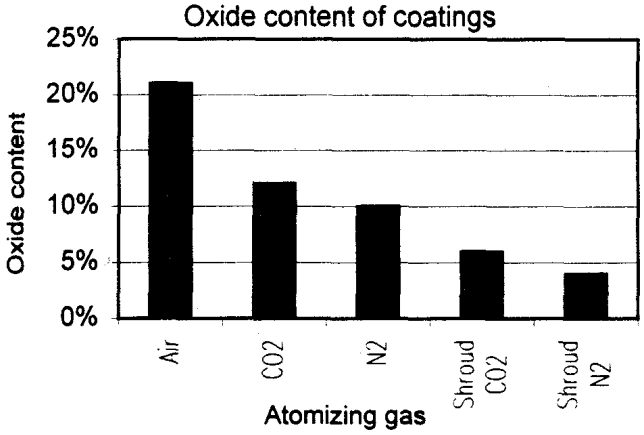

Fig. 14 Oxide content of coatings sprayed with different gases

secondary gas atomization. In this section, the effect of secondary gas injection on adhesion is evaluated.

Sprayed coatings are formed by the impact, deformation, and rapid solidification of individual molten droplets so that their structure consists of a series of overlapping lamellae. The adhesion of the coating depends upon the interactions between individual lamellae and between lamellae and substrate (Ref 16). The bond strength of a coating is affected by the extent of both physical and chemical interactions between the coating and the substrate material and on the microstructure of the interfacial region. Poor adhesion can be attributed to poor interfacial interlocking, low degree of metallurgical bonding, and high internal stresses. The degradation modes of the coating depend on both the nature of the coating-substrate interface and on the chemical phenomena that occur at the interface during deposition and utilization. Therefore, a detailed interface microanalysis could yield interesting information on the role played by interfacial chemistry in coating-substrate adhesion.

The methods of testing coating adhesion of thermally sprayed coatings have been discussed by several other investigators (Ref 17-20). Even though pull-off tensile testing has some limitations, it is acceptable to obtain comparable bond strengths of thermally sprayed coatings. In this study, the bond strength of coatings produced with both nozzles was measured by pull-off tensile tests according to ASTM C 633-79. The interfacial regions were structurally and compositionally studied by SEM, energy dispersive x-ray spectrometry (EDS), and AES to obtain relationships between structure and adhesion. The results of the experiments showed that the bonding mechanism of coating sprayed with secondary gas atomization is not only mechanical but also metallurgical. Figure 15 shows a transition region between coating and substrate. This region was caused by metallurgical bonding. Localized solid interdiffusion, molten mass convection, and interfacial reaction between coating and substrate form an interfacial transition zone. Small amounts of solid solutions and intermetallic compounds formed at the interfacial region, which improved adhesion between coating and substrate.

Bond Strength. The results of tensile adhesion tests (Table 3) indicate that the bond strength of the coating by secondary gas atomization is 40 MPa, while that by primary gas atomization is only 28 MPa.

To reveal the fracture mechanisms of the sprayed coatings, photographs of fracture surfaces were obtained by SEM. In the case of primary gas atomization, the fracture occurred almost entirely along the weakly bonded interface between the coating and substrate. The fracture surface was relatively smooth. It displayed a quasi-cleavage fracture pattern. Coexistence of iron and aluminum peaks in EDS spectra reveal that the fracture mode is failure in the interfacial region. In the case of secondary gas atomization, fracture occurs within the sprayed film. The photograph of the fracture surface shows a dimple fracture pattern, indicating ductile failure. Cracks propagate mainly along unbonded interparticle contact areas and through regions of stress concentration such as pore edges and oxide inclusions within the sprayed film. The only iron peak in the EDS spectra confirms that the failure mode of the sample obtained by the secondary gas atomization is cohesive fracture within the steel coating.

Microstructure and Chemistry of Interface. Figure 15 shows element concentration profiles of coating/substrate cross sections. In the case of primary gas atomization, there is a clear boundary between coating and substrate, while in the case of secondary gas atomization, there exists an intermixed transition zone between deposited coating and substrate. The formation of this intermixed zone can be attributed to metallurgical bonding

Table 3 Bond strength and microhardness of steel coatings from different atomizations (12 measurements)

Atomization type	Bond strength (mean), MPa	Bond strength (σ), MPa	Microhardness (mean), HV	Microhardness (σ), HV
Primary/secondary gas atomization	40.2	6.9	396	15
Primary gas atomization	28.4	5.1	352	13

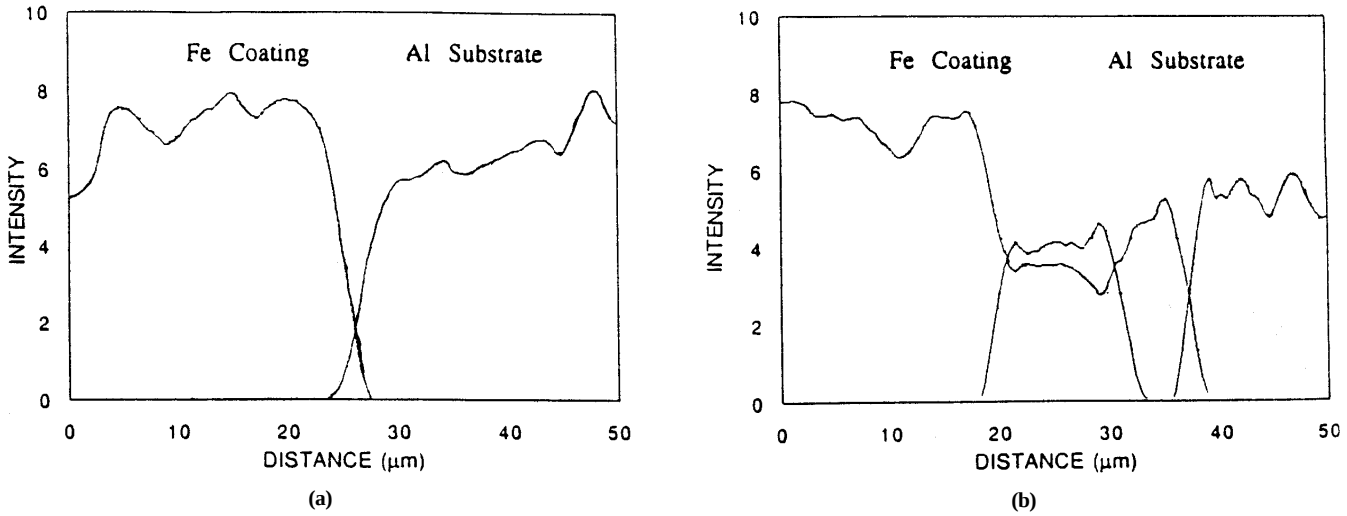

Fig. 15 Element concentration profiles across coating/substrate. (a) Primary gas atomization. (b) Primary/secondary gas atomization

resulting from molten mass convection, solid interdiffusion, and intermediate phase formation.

In the case of secondary gas atomization, the sprayed particles are of small size and mass, have considerably higher velocities, and have higher temperatures according to the situation in the spray jet. They are drastically deformed when striking the substrate surface and have a high cooling rate. The strongest adhesion produced by secondary gas atomization is based on metallurgical interaction between the deposited film and the pretreated substrate. Using secondary gas atomization, particles still remain in the molten state at the instant of impingement on the substrate because of the short flight time. Therefore, the surface of the aluminum substrate will locally melt by heat transfer from the molten particles, and mixing among the liquid phases may occur. Thus, molten substrate metal can infiltrate into porous regions of the deposit. Meanwhile, molten particles can also flow into the cavities of the molten substrate. Successive impingement of molten particles enhances the fluid dynamic mixing. This type of molten mass convection results in localized microwelding of the coating and substrate, which contributes to metallurgical bonding.

When molten particles impinge on the substrate, they spread out, cool down, and solidify at an extremely high quenching rate. The diffusion process which, because of the very short time scale, cannot be described by the classical concepts of diffusion, can be interpreted to be due to the fact that the surface of the substrate has been markedly disturbed by preparatory grit blasting and hence exhibits a high defect concentration. Thus, the molten particles with high temperatures exhibit a high vacancy concentration. Due to this anomalous condition, the interdiffusion process by vacancy-atom interchange can occur with higher diffusion coefficients than is normally the case. Thus, solid interdiffusion also contributes to metallurgical bonding.

Also, intermediate phases are produced during the reaction simultaneously with the diffusion. Energy dispersive x-ray analysis has been carried out on the entire transition zone of the sample cross section, which was deposited by secondary gas atomization. Results indicate that there is a strong elemental mixing in the transition zone. X-ray diffraction analysis was conducted to reveal intermediate phases as shown in Fig. 16. The peaks belonging to Fe_3Al and $FeAl_2$ were visible. The ordered iron-aluminum peak is not clearly identified due to the similarity in d-spacing for certain peaks of the iron and Fe_3Al phases. A further difficulty for identification of iron-aluminum is the peak broadening and peak shifting that occur due to lattice distortion by oversaturated solid solution and thermal stress. Reaction between coating and substrate invariably forms equilibrium phases. At the interfacial region of the secondary gas sprayed steel-aluminum sample, either solid solution or compound formation takes place readily, reaching the lowest free energy composition. The simplest reaction is the formation of a solution of one phase in the other, leading to and maintaining equilibrium saturation in both phases at the interfacial region. A continuation of the reaction is associated with the formation of intermediate phases. The intermetallic compounds formed during reactions are compatible with both phases at the coating and the substrate. Several recent studies have shown that the mechanical properties of heterophase interfaces can be controlled by interfacial reactions (Ref 21, 22). Introducing either intermetallic compounds or solid solutions in the transition zone can increase the strength of the interface between coating and substrate.

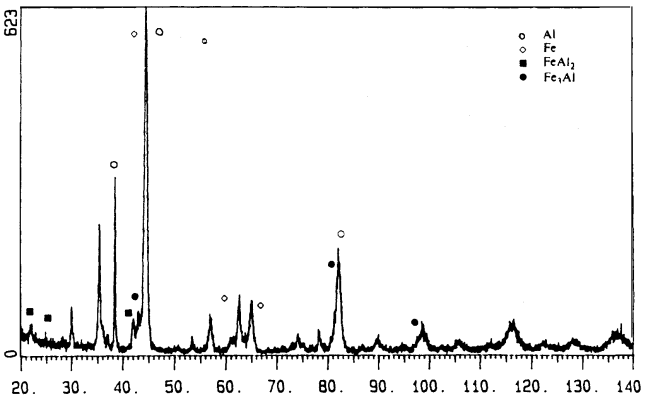

Fig. 16 X-ray diffraction pattern of interfacial region of sample sprayed with primary/secondary gas atomization

Adhesion Mechanisms. Secondary gas sprayed stainless steel coatings on aluminum substrates reveal higher bonding strength than those sprayed with only primary gas. Failure occurs preferentially within the deposited film due to its stronger interfacial strength. The following three types of bonding mechanisms are operative in spraying with secondary gas atomization:

- Physical bonding: The action of van der Waals forces between coating and substrate
- Mechanical bonding: A molten particle striking a roughened substrate surface, given that it has sufficient fluidity, will assume the surface topography. Mechanical interlocking between the protrusions of the deposit and the roughened substrate leads to mechanical adherence. Higher velocity and temperature of the particles in secondary gas atomization enhance mechanical bonding.
- Metallurgical bonding: In secondary gas atomization, adhesion improvement could be due to metallurgical bonding caused by melt convection, interdiffusion, and intermetallic phase formation.

4. Conclusions

The following conclusions can be drawn:

The fluid dynamic design of wire arc spray nozzles has a strong influence on the coating characteristics, and coating properties can be improved by relatively minor modifications of the spray gun design. Higher gas velocities at the wire tip location can be achieved either by shaping the atomizing gas nozzle such that proper expansion of the flow reduces the formation of shocks, or by the introduction of a secondary gas in a plenum upstream of the wire guides. While use of air as atomizing gas results in increased oxidation when the particle size is reduced, using nonoxidizing gases such as nitrogen or carbon dioxide in combination with a shroud can minimize this oxidation. The higher gas velocities and the associated smaller particle sizes and higher particle velocities result in higher density coatings and improved adhesion of the coatings. This improved adhesion can be attributed to the formation of metallurgical bonds, which have been observed when the particle velocity and temperature

at impact are sufficiently high. Under these conditions, failure occurs within the film rather than at the interface.

Acknowledgment

This study was supported in part by the NSF through the Engineering Research Center for Plasma-Aided Manufacturing, grant No. EEC 8721545. The government has certain rights in this work.

References

1. *Thermal Spraying: Practice, Theory and Applications*, Committee on Thermal Spraying, American Welding Society, Miami, FL, 1985, p 3-12
2. H.-D. Steffens, Z. Babiak, and M. Wewel, Recent Developments in Arc Spraying, *IEEE Trans. Plasma Sci.*, Vol 18 (No. 6), 1989, p 974
3. M.L. Thorpe, Thermal Spray Applications Grow, *Adv. Mater. Process.*, Vol 134 (No. 4), 1988, p 69
4. H.-D. Steffens, Metallurgical Changes in the Arc Spraying of Steel, *Br. Weld. J.*, Vol 13 (No. 10), 1966, p 597-605
5. R.W. Fox, *Introduction to Fluid Mechanics*, John Wiley & Sons, 1973, p 54
6. S.G. Russ, "Turbulence and Entrainment in Plasma and Heated Jets," Ph.D. thesis, University of Minnesota, 1993
7. David R. Marantz and Daniel R. Marantz, State of the Art Arc Spray Technology, *Thermal Spray Research and Applications*, T.F. Bernecki, Ed., ASM International, 1990, p 113
8. K.S. Fessenden and Z. Zurecki, Sliding Wear Resistance of Electric Arc Sprayed Coatings, *Thermal Spray Research and Applications*, T.F. Bernecki, Ed., ASM International, 1990, p 81
9. X. Wang, D. Zhuang, E. Pfender, J. Heberlein, and W. Gerberich, Effect of Atomizing Gas Pressure on Coating Properties in Wire Arc Spraying, *Thermal Spray Industrial Applications*, C.C. Berndt and S. Sampath, Ed., ASM International, 1994, p 587-592
10. T. Watanabe, X. Wang, J. Heberlein, E. Pfender, and W. Herwig, Voltage and Current Fluctuations in Wire Arc Spraying as Indications for Coating Properties, *Thermal Spray: Practical Solutions for Engineering Problems*, C.C. Berndt, Ed., ASM International, 1996, p 577-583
11. E. Pfender, Plasma Jet Behavior and Modeling Associated with the Plasma Spray Process, *Thin Solid Films*, Vol 238, 1994, p 228-241
12. X. Wang, S. Russ, J. Heberlein, W. Gerberich, and E. Pfender, Arc Spray by a Supersonic Atomizing Gas Stream, *Proceedings of the 11th International Symposium on Plasma Chemistry* (Leicestershire, England), J. Harry, Ed., Vol 1, 1993, p 133
13. A.W. Schrader, *Modern Approaches to Wettability, Theory and Applications*, Plenum Press, 1992, p 41-45
14. X. Wang, J. Heberlein, E. Pfender, and W. Gerberich, Effect of Shrouded CO_2 Gas Atomization on Coating Properties in Wire Arc Spray, *Thermal Spray Science and Technology Proceedings*, C.C. Berndt and S. Sampath, Ed., ASM International, 1995, p 31-37
15. N. Birks and G. Meier, *Introduction to High Temperature Oxidation of Metals*, Edward Arnold Ltd., London, 1983, p 67
16. H. Herman, Plasma Sprayed Coatings, *Sci. Am.*, Vol 45 (No. 7), 1988, p 112-117
17. C.C. Berndt, Instrumental Tensile Adhesion Tests on Plasma Sprayed Barrier Coatings, *J. Mater. Eng.*, Vol 11 (No. 4), 1989, p 275
18. H.-D. Steffens, D. Wielage, and J. Drozak, Interface Phenomena and Bonding Mechanism of Thermally Sprayed Metal and Ceramic Composites, *Surf. Coat. Technol.*, Vol 45 (No. 3), 1991, p 299
19. C.C. Berndt, The Need for Standardization of Testing Techniques in Thermal Spray Industry, *Thermal Spray Research and Applications*, T. Bernecki, Ed., ASM International, 1990, p 325
20. C.C. Berndt and R. McPherson, Adhesion of Plasma Sprayed Ceramic Coatings to Metals, *Mater. Sci. Res.*, Vol 14 (No. 3), 1983, p 619
21. F.S. Shieu, R. Raj, and S.L. Sass, Control of the Mechanical Properties of Metal-Ceramic Interfaces through Interfacial Reactions, *Acta Metall. Mater.*, Vol 38 (No. 11), 1990, p 2215
22. R. Raj, A. Pearce, and C.M. Kennefick, Thin Films of Transition Metals on Oxides, *Acta Metall. Mater.*, Vol 38 (No. 11), 1990, p 2215